Neuron
Article

Neuronal Elav-like (Hu) Proteins Regulate RNA Splicing and Abundance to Control Glutamate Levels and Neuronal Excitability

Gulayse Ince-Dunn,[1,5] Hirotaka J. Okano,[3] Kirk B. Jensen,[1,6] Woong-Yang Park,[1,7] Ru Zhong,[1] Jernej Ule,[1,8] Aldo Mele,[1] John J. Fak,[1] ChingWen Yang,[1] Chaolin Zhang,[1] Jong Yoo,[4] Margaret Herre,[1] Hideyuki Okano,[3] Jeffrey L. Noebels,[4] and Robert B. Darnell[1,2,*]

[1]Laboratory of Molecular Neuro-Oncology
[2]Howard Hughes Medical Institute
The Rockefeller University, 1230 York Avenue, New York, NY 10021, USA
[3]Keio University School of Medicine, 1058461 Tokyo, Japan
[4]Departments of Neurology, Neuroscience, and Molecular and Human Genetics, Baylor College of Medicine, One Baylor Plaza, Houston, TX 77030, USA
[5]Current address: Department of Molecular Biology and Genetics, Koç University, Istanbul 34450, Turkey
[6]Current address: School of Molecular and Biomedical Science, The University of Adelaide, Adelaide SA 5005, Australia
[7]Current address: Department of Biomedical Sciences, Seoul National University College of Medicine, Seoul 110-799, Korea
[8]Current address: Medical Research Council (MRC) Laboratory of Molecular Biology, Cambridge CB2 0QH, UK
*Correspondence: darnelr@rockefeller.edu
http://dx.doi.org/10.1016/j.neuron.2012.07.009

SUMMARY

The paraneoplastic neurologic disorders target several families of neuron-specific RNA binding proteins (RNABPs), revealing that there are unique aspects of gene expression regulation in the mammalian brain. Here, we used HITS-CLIP to determine robust binding sites targeted by the neuronal Elav-like (nElavl) RNABPs. Surprisingly, nElav protein binds preferentially to GU-rich sequences in vivo and in vitro, with secondary binding to AU-rich sequences. nElavl null mice were used to validate the consequence of these binding events in the brain, demonstrating that they bind intronic sequences in a position dependent manner to regulate alternative splicing and to 3′UTR sequences to regulate mRNA levels. These controls converge on the glutamate synthesis pathway in neurons; nElavl proteins are required to maintain neurotransmitter glutamate levels, and the lack of nElavl leads to spontaneous epileptic seizure activity. The genome-wide analysis of nElavl targets reveals that one function of neuron-specific RNABPs is to control excitation-inhibition balance in the brain.

INTRODUCTION

The regulation of posttranscriptional gene expression increases organismal complexity and proteome diversity in higher organisms. Not surprisingly such regulation, including alternative splicing (AS), 3′UTR regulation and RNA editing is especially prevalent in the nervous system, likely underlying the complex set of reactions carried out in this tissue required for the development and physiology of the many different cell types in the brain (Castle et al., 2008; Li et al., 2007, 2009; Licatalosi and Darnell, 2010; Pan et al., 2008; Wang et al., 2008). Tissue-specific AS and 3′UTR regulation are regulated by the interactions of *cis*-acting elements on RNA with RNA binding proteins (RNABPs) that bind to and either block or enhance the recruitment of the regulatory machinery. New technologies to assess tissue-specific AS have rapidly expanded (Barash et al., 2010; Calarco et al., 2011; Castle et al., 2008; Das et al., 2007), revealing new rules of regulation, such as the finding that the position of RNABP binding within a pre-mRNA is a major determinant of AS control (Licatalosi and Darnell, 2010).

Although a very large fraction of RNABPs encoded in the mammalian genomes are expressed in the nervous system, their RNA targets and the roles of these targets in neuronal physiology are largely unknown (McKee et al., 2005). One such highly abundant family of RNABPs are the *Elavl* (Elav-like) genes that share significant homology with the *Drosophila ELAV* (embryonic *l*ethal and *a*bnormal *v*ision) gene. *Elavl1* (HuA/R) is expressed in a wide range of non-neuronal tissues and has been reported to regulate various gene expression processes in tissue culture cells, including regulation of steady state levels by binding to ARE (AU-rich elements) in 3′UTRs of target mRNAs (Brennan and Steitz, 2001; Hinman and Lou, 2008). Three other family members, Elavl2 (HuB/Hel-N1), Elavl3 (HuC), and Elavl4 (HuD) were discovered as autoantigens in a multisystem neurologic disorder termed paraneoplastic encephalomyelopathy (Szabo et al., 1991), and are exclusively expressed in neurons (referred to collectively as neuronal Elavl [nElavl]) (Okano and Darnell, 1997). The nElavl proteins exhibit a high degree of sequence homology and structural similarity with the well-established *Drosophila* AS factor SXL (Sex-lethal) as well as ELAV (Koushika et al., 1996, 2000; Lisbin et al., 2001; Soller and White, 2003, 2005; Wang and Bell, 1994). More recently, several studies

carried out in mammalian cell lines have presented evidence that the nElavl proteins are able to regulate alternative splicing of several pre-mRNAs (Hinman and Lou, 2008; Lebedeva et al., 2011; Mukherjee et al., 2011; Wang et al., 2010a; Zhu et al., 2008). However, it is not known whether and to what extent nElavl proteins are regulators of AS in vivo in the mammalian nervous system. Moreover, the range of endogenous target RNAs of nElavl proteins and the kinds of neuronal processes regulated by these targets are unknown, other than a compilation of RNAs coprecipitating with Elavl4 (HuD) in transgenic Elavl4 overexpressing mice (Bolognani et al., 2010).

Generating RNA profiles that compare WT and mutant animals has provided a powerful means of correlating RNA variants with the action of RNABPs, but such strategies are unable to discriminate direct from indirect actions. Combining such data with global maps of direct RNABP-RNA interaction sites can generate unbiased genome-wide insight into the regulation of alternative splicing (Licatalosi and Darnell, 2010). This has been accomplished by applying cross-linking and immunoprecipitation methods (Jensen and Darnell, 2008; Ule et al., 2003, 2005a), particularly in combination with high-throughput sequencing (HITS-CLIP) (Licatalosi et al., 2008), to analyze in vivo RNABP-RNA interactions (Darnell, 2010). HITS-CLIP was first used to identify hundreds of transcripts that are directly regulated by the neuronal RNABP Nova in the brain (Licatalosi et al., 2008) and has subsequently been used to analyze RNA regulation mediated by a number of RNABPs (Darnell et al., 2011; König et al., 2010; Lebedeva et al., 2011; Mukherjee et al., 2011; Tollervey et al., 2011; Xue et al., 2009; Yeo et al., 2009). Combining such analyses has yielded significant insight into the role of Nova in neuronal physiology, development and disease (Huang et al., 2005; Ruggiu et al., 2009; Yano et al., 2010).

In this study, we have generated *Elavl3* null mice and used splicing-sensitive microarrays and deep RNA sequencing to identify nElavl-dependent regulatory events, and overlaid this analysis with nElavl HITS-CLIP maps. Our results indicate that in neurons, nElavl preferentially binds to conserved U-rich sequences interspersed with G residues at exon-intron junctions to either repress or enhance the inclusion of alternative exons. These data were used to generate a position-dependent map of nElavl functional binding sites in AS regulation and to discover that while nElavl regulates largely independent gene networks through overall transcript level and AS, these intersect in the control of the synthesis of the major excitatory neurotransmitter glutamate. In the absence of nElavl proteins, the level of glutamate is severely compromised, and this imbalance is associated with seizures in *Elavl3* null mice. Taken together our genome-wide approaches identify in vivo targets and functions of nElavl proteins in regulating brain RNA and excitability.

RESULTS

Generation of *Elavl3* Knockout Mice

To assess the functional action of Elavl3 on target transcripts, we first generated an *Elavl3* null mouse by homologous recombination in ES cells (Figure 1A). Mice harboring the homologous recombinant cassette made no detectable Elavl3 by either RNA or protein analysis, including western blot and immunofluorescence microscopy (Figure 1B and data not shown). $Elavl3^{-/-}$ mice were viable and fertile. However, when they were inbred into a C57Bl/6 background, we noted that $Elavl3^{-/-}$ mice were present in new litters at well-below Mendelian ratios (~10% offspring from the mating of two heterozygous parents). Interestingly, when $Elavl3^{-/-}$ mice were outbred into the CD1 strain, $Elavl3^{-/-}$ pups were born at Mendelian ratios, suggesting gene modifiers present in the outbred CD1 strain.

We contrasted nElavl immunofluorescence remaining in $Elavl3^{-/-}$ mouse brain with previously characterized *Elavl3* expression characterized by in situ hybridization (Okano and Darnell, 1997). In particular, we had previously noticed that several neuronal types showed nearly exclusive expression of *Elavl3* among all nElavl isoforms, including cerebellar Purkinje neurons and hippocampal dentate gyrus (DG) neurons. Immunofluorescence microscopy using a pan-nElavl antibody revealed the absence of detectable remaining nElavl protein in both Purkinje and DG neurons in the $Elavl3^{-/-}$ brain (Figures 1D and 1E), consistent with Elavl3 being the sole nElavl protein in these neurons.

Given that all nElavl expression was eliminated in $Elavl3^{-/-}$ Purkinje neurons, we decided to analyze cerebellar function in these mice by rotarod assay. This behavioral assay is widely used to evaluate cerebellar dysfunction; however, other explanations to reduced time on rotating rod are potentially possible. Young adult $Elavl3^{-/-}$ mice showed significant defects in this assay ($p = 0.001$) relative to heterozygous littermates (Figure 1C). In order to exclude a generalized synaptic dysfunction in these mice, we measured time to tail-twitch on hotplate testing as a measure of sensory function and observed no difference in either genotype, consistent with the observation that Elavl2, 3, and 4 are all robustly expressed in dorsal root ganglia (Okano and Darnell, 1997). Taken together, these observations suggest that there are subsets of neurons that are particularly vulnerable to the loss of Elavl3, while others are relatively resistant, consistent with the expression patterns of the individual family members and functional redundancy among nElavl proteins. We also did not detect any gross anatomical defects in the $Elavl3^{-/-}$ brain that could have potentially caused nonspecific phenotypic effects (data not shown).

Whole Genome High-Throughput Sequencing of nElavl-Bound RNA

In order to purify target RNA molecules to which nElavl proteins are directly bound in vivo we carried out HITS-CLIP with three different anti-nElavl antisera (each of which was specific for the nElavl proteins; see Figure S1A available online). Six independent CLIP experiments using WT and four independent experiments using $Elavl3^{-/-}$ cortical tissue were completed (Figures 2A–2D). As a negative control, immunoprecipitation was carried out using two different unrelated control antibodies that recognized cdr2/3 proteins (anti-Yo antisera). We also examined dependence on UV crosslinking by immunoprecipitating nElavl from noncrosslinked tissue. In both of these controls, no signal was detected after radio-labeling the immunoprecipitated RNA and analyzing the results by denaturing PAGE (Figure 2E).

Out of 26,190,453 total reads, we obtained 11,966,926 reads that can be unambiguously mapped to unique loci of the

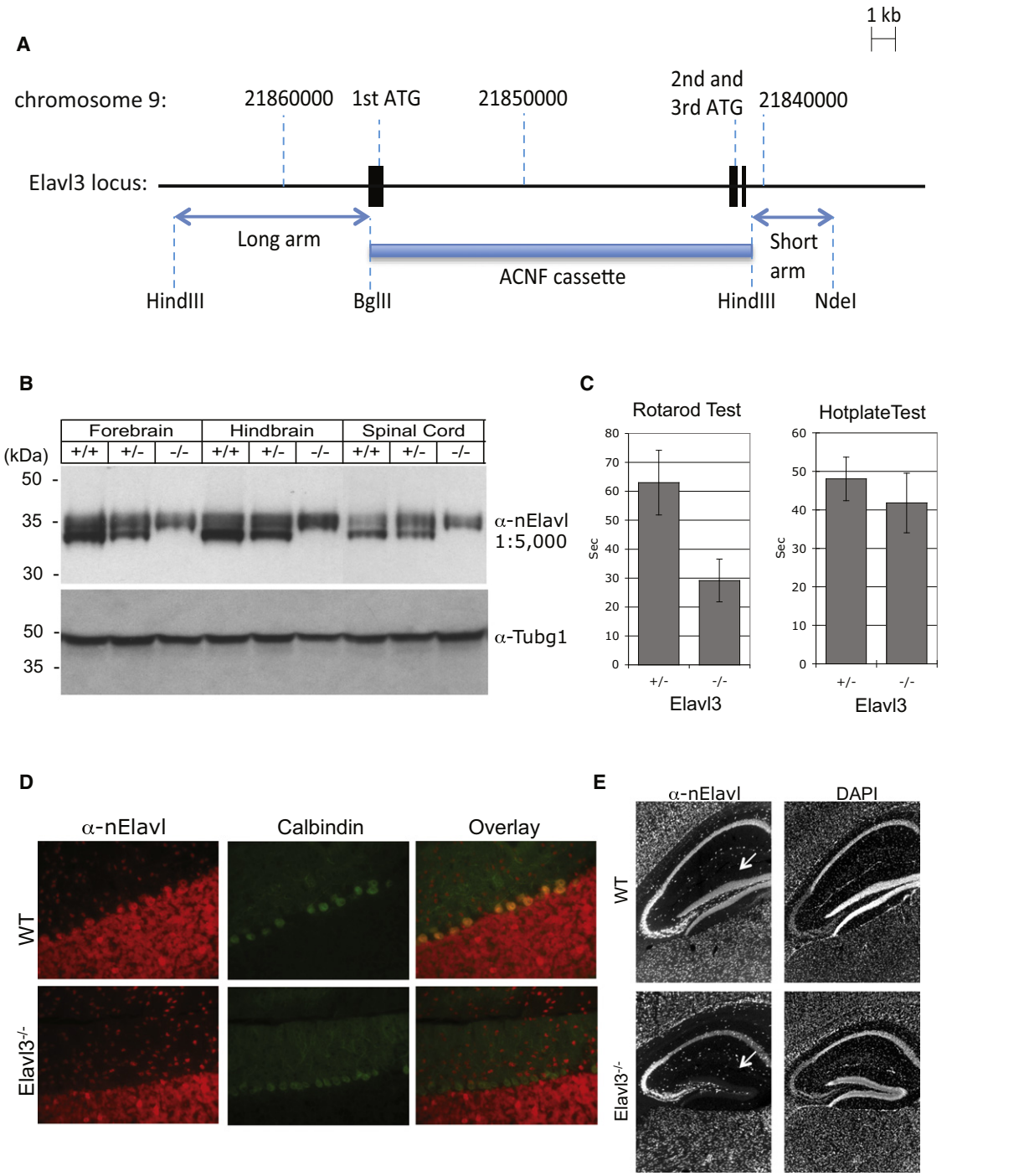

Figure 1. Generation of *Elavl3*$^{-/-}$ Knockout Mice

(A) The targeting construct used in generating *Elavl3* KO locus by homologous recombination.

(B) The expression of Elavl3 protein is abolished in *Elavl3*$^{-/-}$ brain tissue (P21 WT, heterozygote and KO mice [littermates], as indicated). The lower heavy band corresponds to Elavl3, upper bands represent Elavl2 and Elavl4. Results from P21 WT, *Elavl3*$^{+/-}$, and *Elavl3*$^{-/-}$ mice were repeated in three independent litters.

(C) Rotarod or hotplate testing of cerebellar or sensory physiology in *Elavl3*$^{+/-}$ or *Elav3*$^{-/-}$ littermates, as indicated; second until falling off the rod or tail twitch are shown. Rotarod testing was done with 6∼8-week-old males (n = 3; $p < 0.0001$), and hotplate testing was done with 7∼9-week-old males (n = 3, $p = 0.11$). Error bars denote standard deviation.

(D and E) IF microscopy of *Elavl3*$^{-/-}$ mice compared to WT (+/+) littermate controls. A pan anti-nElavl antibody (α-nElavl) was used for IF and contrasted with staining for the Purkinje neuronal marker Calbindin (D) or nuclei (DAPI, E).

(E) Arrows point to nElavl immunostaining in WT and lack of it in *Elavl3*$^{-/-}$ DG.

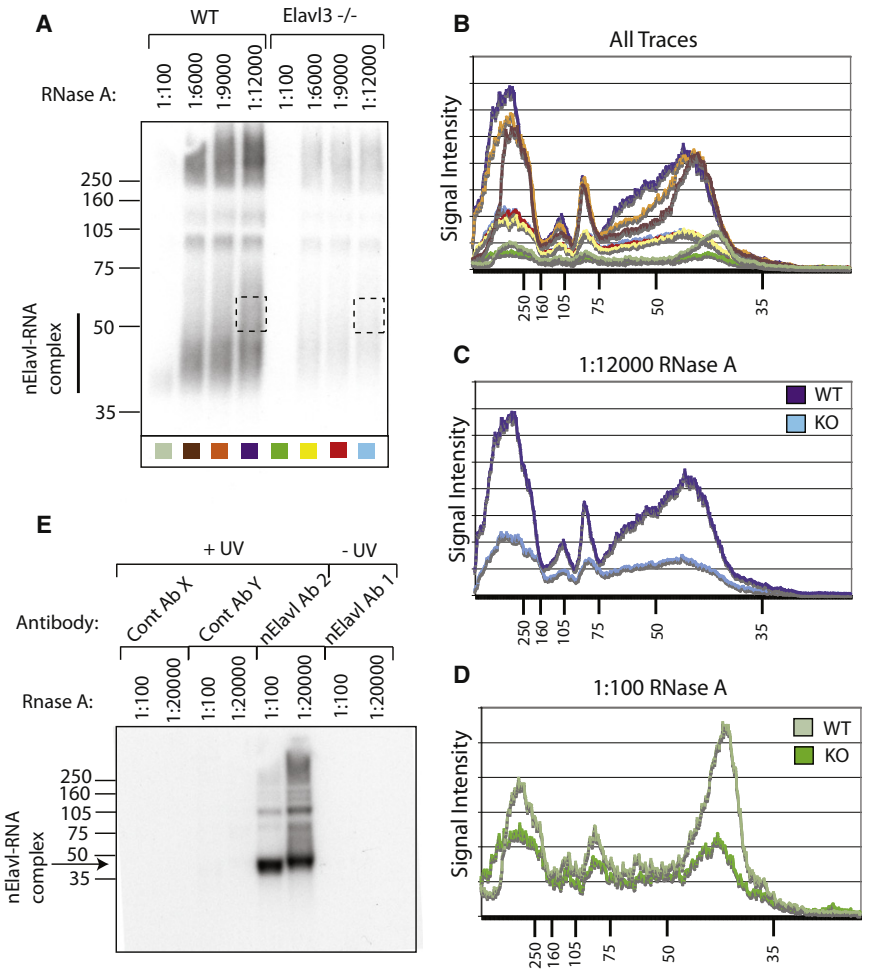

Figure 2. Isolation of nElavl-RNA Complexes by CLIP

(A) nElavl-RNA complexes from WT and *Elavl3*$^{-/-}$ forebrain tissue from mice at age P0 were UV-crosslinked and immunoprecipitated (by nElavl antibody1) using the CLIP method. Representative autoradiograms of [γ-^{32}P]ATP 5′end labeled RNA molecules, run on a polyacrylamide gel and blotted onto nitrocellulose filter are shown. Over-digestion of the lysate with RNase A (1:100 dilution) resulted in approximately a 40 kDa band, corresponding to nElavl and associated RNA fragments that are protected. The size of nElavl-associated RNA was titrated by increasing dilutions of RNase A treatment. Stronger signal was detected in the WT lanes as opposed to *Elavl3*$^{-/-}$ lanes. The signal detected in the *Elavl3*$^{-/-}$ lanes are due to Elavl2/4 that are also immunoprecipitated by the same antibody. Hatched box marks the piece of membrane from which nElavl-associated RNA was isolated.

(B–D) Line traces of nElavl-RNA membrane shown in (A) are plotted. Individual lanes are color coded.

(E) No signal was detected when two different control antibodies (anti-Yo autoantibodies) were used (lanes 1–4) or when UV-crosslinking was omitted (lanes 7–8). nElavl-RNA complexes have been immunoprecipitated using antibody2 (lanes 9–10).

See also Figure S1 and Tables S1–S3.

reference genome (mm9) (Table S1). Further collapsing of potential PCR duplicates by identical genomic coordinates gave 822,933 unique reads (nElavl tags) belonging to 81,468 clusters (Tables S1 and S2) (a group of two or more tags overlapping by at least one nt [nucleotide]). In order to determine a set of statistically significant reproducible clusters, for each cluster we calculated a biological complexity coefficient (BC), representing the number of independent experiments that contributed tags to the corresponding cluster, a chi-square score and a false discovery rate (Table S2). To assess differences in the specificity of three different nElavl antibodies, we determined correlation coefficients (R^2) between individual experiments. A high correlation was evident in all pair-wise comparisons of antibodies and in comparison of clusters in WT and *Elavl3*$^{-/-}$ tissue when we calculated R^2 coefficients based on number of tags per 3′UTRs of individual genes (Ab1-Ab1: 0.83 (2 independent experiments), Ab1-Ab2: 0.8, Ab1-Ab3: 0.79, WT-*Elavl3*$^{-/-}$: 0.81). In contrast, comparison of nElavl clusters with those of another neuronally expressed RNA binding protein, Nova (Licatalosi et al., 2008), resulted in a R^2 value of only 0.28, demonstrating the specificity and consistency of CLIP results using individual nElavl antibodies. We also calculated R^2 values based on number of tags in individual clusters. Since this is a more stringent method of calculation in general we observed lower R^2 values (Table S3). Nonetheless, a higher correlation between the three nElavl antibodies in comparison to nElavl and Nova tags was evident.

To gain insight into the potential functional roles nElavl proteins have in RNA regulation, we determined the location of nElavl clusters on target RNA molecules. Analysis of reproducible binding sites with no winnowing of data (all 81,468 clusters) demonstrated that the majority (68.3%) mapped to mRNA-encoding genes, while many (31.7%) mapped to intergenic regions, which may correspond to bona fide binding in unannotated RNAs or may represent biologic or experimental noise. To focus on highly reproducible mRNA clusters, we identified clusters that harbored CLIP tags from at least five out of six independent experiments (BC = 5/6 or 6/6). Interestingly, the vast majority of these reproducible clusters were in the 3′UTR, with very few reproducible 5′UTR clusters and relatively few intronic clusters. For example, among 747 clusters with BC $\geq$ 5/6, 74% mapped to the 3′UTR (including sequences within 10 kB downstream of stop codons, which most likely correspond to unannotated 3′UTRs) (Licatalosi et al., 2008), while only 12% mapped to introns and only one mapped to the 5′UTR (Figure 3A). A very similar distribution profile of clusters was evident in the results obtained from *Elavl3*$^{-/-}$ tissue. Taken together, our results suggest a possible role for nElavl proteins in the regulation of pre-mRNA and also indicate that the greatest steady-state binding to defined sites is in neuronal 3′UTRs.

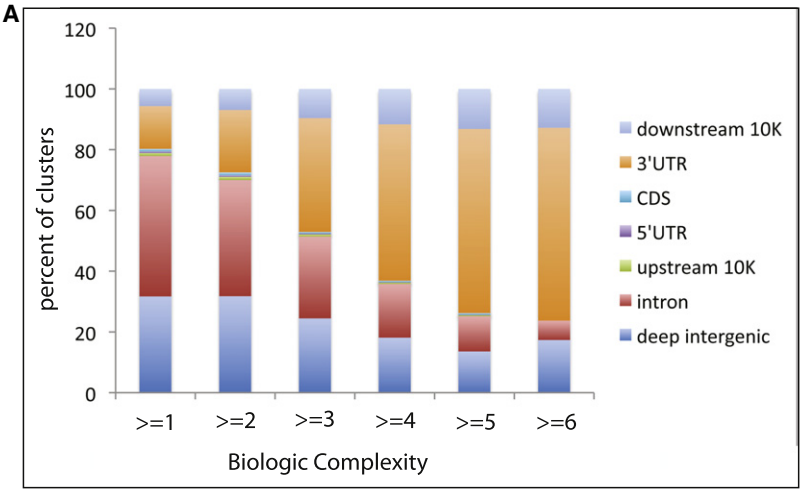

B

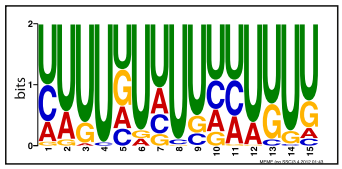

C

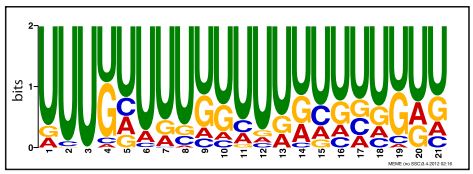

D

10 most frequent hexamers	Number of observations
UUUUUU	529
UUGUUU	164
UUUUGU	162
AUUUUU	161
UGUUUU	157
UUUGUU	156
UUUUUA	142
UUAUUU	141
UUUUUG	139
UAUUUU	138

Figure 3. nElavl Binds to U-rich Sequences

(A) Distribution of nElavl tag clusters generated from six independent WT tissue samples is plotted as a function of biologic complexity.

(B and C) Cluster sequences with either FDR < 0.01 (B) or BC > = 1 (C) were used to predict nElavl binding motif by MEME-CHIP tool.

(D) Top ten most frequent hexamers found in nElavl clusters (FDR < 0.01).

See also Tables S4–S6.

In order to gain insight into Elavl3 only clusters and hence Elavl3-dependent biological functions we subtracted clusters obtained using *Elavl3*$^{-/-}$ tissue from WT clusters. The subtracted data set (presumably representing Elavl3 only clusters) as well as the WT data set were most significantly enriched in genes regulating synaptic function, postsynaptic membrane, neuronal transmission, and glutamate receptor activity. The *Elavl3*$^{-/-}$ data set (presumably representing Elavl2/4 only clusters) was most significantly enriched in genes regulating neuronal projections, dendrites, and axons. This set was also enriched in genes that regulate RNA binding, a feature that we did not observe in the subtracted data set. These data suggest that synaptic function might be preferentially regulated by Elavl3 as opposed to Elavl2 or 4 (Table S4).

We determined the consensus nucleotide sequence preference of nElavl binding to target RNA from our CLIP data. The nucleotide sequences of 238 most robust cluster sites (FDR < 0.01) were analyzed by MEME-CHIP tool designed for generating consensus motifs using large data sets (Bailey and Elkan, 1994). The most frequent (159/238) and significant (E value: 14e^{-106}) motif was a 15 nt long sequence enriched in U nucleotides (Figure 3B). We also analyzed the sequence preference of all clusters (BC $\geq$ 1) representing a larger data set with lower confidence and similarly observed a U-rich motif with a secondary preference for G nucleotides (Figure 3C).

Next, we analyzed the frequency of all possible hexameric sequences within the robust clusters (FDR < 0.01 or BC $\geq$ 5). We carried our analysis in different subsets of clusters depending on where the clusters were located on individual transcripts (i.e., 3′UTRs, 5′UTRs, coding regions, or introns) to determine whether there were different sequence preferences for nElavl-binding to different locations on a pre-mRNA. In all subsets, we observed a general trend where the majority of hexamers among the most frequently identified, consisted of a stretch of pure U residues (28% of top ten most frequent hexameric sequences identified in clusters with FDR < 0.01) or a U stretch embedded mostly with a single G (41%) and to a lesser extent a single A nucleotide (31%) (Figure 3D). Often we observed a stretch of A residues in the top ten most frequent hexameric sequences, which we believe represents an artifact of sequencing and were removed from further analysis (Table S5).

The CLIP binding consensus was somewhat unexpected, as the nElavl proteins were originally suggested to bind more specifically to AU-rich elements in vitro or in tissue culture cells (Table S6), while GU-rich elements were ~1.3-fold more abundant that AU-rich elements in nElavl binding clusters. We therefore compared the CLIP results with in vitro RNA selection undertaken with the nElavl proteins. Recombinant histidine-tagged Elavl2, 3, and 4 proteins were purified and used for in vitro RNA selection using column chromatography to select from a random library of 52 nt RNAs (complexity 10^{15}, as previously described in Buckanovich and Darnell [1997]). After seven rounds of in vitro selection, bound RNAs were sequenced, revealing a consensus in which nElavl bound U-rich stretches interspersed with purine residues, primarily G residues (Figure 4A). We confirmed that Elavl4 directly bound these RNAs with high-affinity (Kd ~1.5–4.5 nM) by gel shift and filter binding assays (Figures 4B and 4C). Such concordance of in vitro RNA selection and in vivo CLIP data has also been seen in comparison of Nova CLIP and RNA selection data (Zhang et al., 2010)

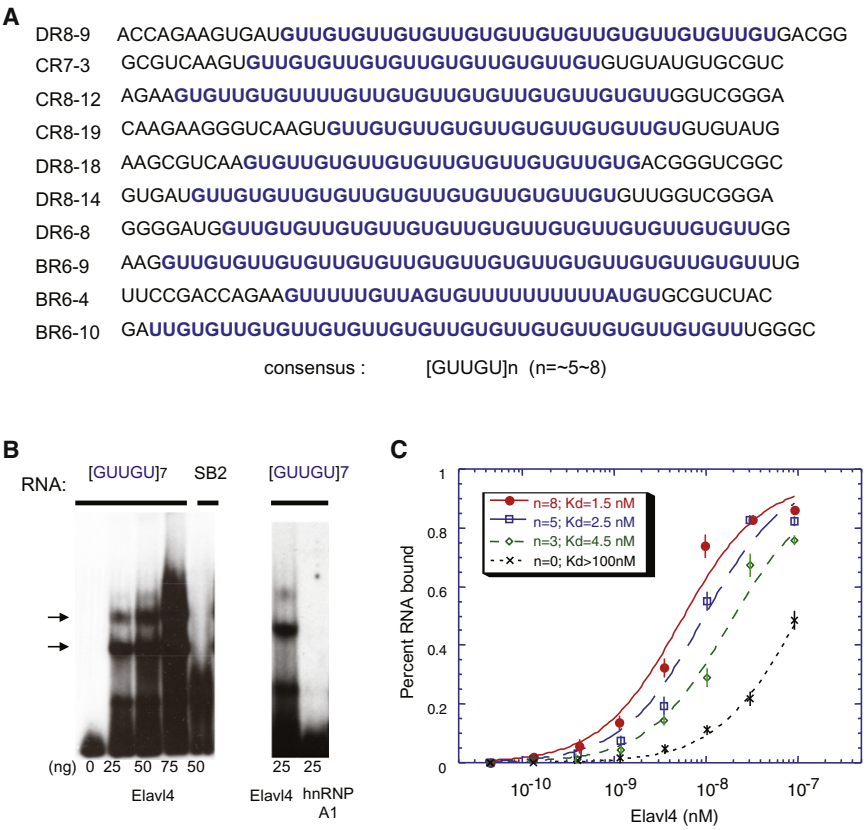

Figure 4. In Vitro Selection of nElavl Binding RNA Molecules

(A) Representative results from in vitro RNA selection with the nElavl proteins. RNA selection was carried out using the Elavl2, Elavl3, or Elavl4 proteins for 6–8 rounds of selection (R6–R8, as indicated). Consensus GU-rich elements are shown in blue and below the diagram.

(B) RNA gel-shift assay, in which DR8-9 clone RNA selected by Elavl4 was incubated with recombinant Elavl4 as indicated. Multiple forms of Elavl4/RNA complexes (arrows) have slower migration profiles with increasing amounts of protein (RNA = 50 fmol/lane, protein = 0, 25, 50, or 75 ng), and this effect is specific, as no effect on RNA mobility was seen with either hnRNP A1 (25 ng) or when Elavl4 was incubated with an irrelevant control RNA (SB2, a 52 base NOVA1 consensus sequence).

(C) Results of filter binding assays in which the indicated amounts of Elavl4 fusion protein were incubated with radiolabeled selected RNA (where the number of GUUGU repeats [n] is shown, see A). Red, DR8-2 RNA; blue, DR8-15 RNA; green, DR7-5 RNA; black, control SB2 RNA (50 fmol/reaction). Estimated kDs are shown. Error bars denote standard deviation.

and suggests that nElavl proteins function in vivo by binding to clustered U-rich sequences, with interspersed purine residues (G > A).

Analysis of nElavl-Dependent Alternative Splicing in the Brain

The finding that nElavl binds to specific intronic sequences suggested that the proteins might have roles in neuronal alternative splicing. To investigate this possibility a whole genome analysis of alternative splicing was undertaken. Given evidence of nElavl functional redundancy among nElavl paralogs and previous findings of quantitatively larger (albeit qualitatively similar) splicing defects in Nova1/2 DKO pups (Ule et al., 2006) relative to single Nova null mice (Ule et al., 2005b), we generated *Elavl3*$^{-/-}$;*Elavl4*$^{-/-}$ DKO mice for splicing analyses (Akamatsu et al., 2005). These mice were born alive and were initially indistinguishable from WT littermates but died several hours after birth. Elavl3 is the major nElavl homolog expressed in the cortex at age P0 and deletion of *Elavl3* and *Elavl4* together results in loss of approximately 65% of total nElavl proteins in the cortex (Figure S1B). Since *Elavl3/4* DKO pups die at P0, this time point was chosen for analysis of splice isoforms of RNA transcripts. Further, at time P0 nElavl protein levels are very close to the peak expression observed at P7 in the cortex (Figure S1C).

Total RNA samples isolated from *Elavl3*$^{-/-}$;*Elavl4*$^{-/-}$ DKO and WT cortex at age P0 was profiled by exon junction microarrays. Results were analyzed using an updated version of the ASPIRE algorithm that identifies reciprocal changes in exon-excluded versus exon-included mRNA isoforms (Licatalosi et al., 2008; Ule et al., 2005b). These analyses identified 227 alternative exons with significant splicing changes (according to a modified t test, $|\Delta I\text{-rank}| > 10.0$; see Experimental Procedures). RT-PCR was used to test and validate 15 out of 17 of these alternative splicing events with $|\Delta I|$ values (the absolute value of the change in fraction of alternative exon usage) higher than 0.15. We additionally screened 36 more targets with lower $|\Delta I|$ values and validated an additional 22 targets. In total, 37 targets were verified with experimentally validated $|\Delta I|$ values between 0.05 and 0.44 (Tables 1 and S7; Ule et al., 2005b). Among these, 24 validated AS events displayed increased exon exclusion and 13 displayed increased exon inclusion in *Elavl3*$^{-/-}$;*Elavl4*$^{-/-}$ mouse cortex. Within the validated AS events, we observed predominantly cassette-type alternative exon usage, as well as alternative 5′ and 3′ splice site choice, mutually exclusive exon usage, and other complex patterns of alternative splicing (Tables 1 and S7). Although quantitatively smaller, a large fraction of these alternatively spliced exons also exhibited changes in relative isoform abundance in single *Elavl3* KOs but not in single *Elavl4* KOs (Table S7).

Generation of nElavl-RNA Regulatory Map

The finding that some exons are misregulated in *Elavl3*$^{-/-}$;*Elavl4*$^{-/-}$ brain suggests that the nElavl proteins might be regulating splicing directly. To examine whether this was the case, and whether the position of nElavl binding also might determine the outcome of splicing, we overlaid a nElavl binding map on the set of Elavl3/4 regulated cassette exons. We analyzed 59 cassette-type alternative exons that were either validated by RT-PCR or predicted based on a t test ranking of Aspire2

Table 1. List of All Verified Elavl3/4-Dependent Alternative Exons

Gene Symbol	Transcript Level Change	Alt Exon Coordinates (mm 9)	Alt Splicing Event	ΔI (Microrray)	ΔI (RT-PCR)
Clip1	1.01	chr5:124077303-124077419	cassette/complex	−0.3	−0.44
Camta1	1.14	chr4:151166528-151166611	intron retention	−0.38	−0.39
Grip1	0.98	chr10:119422530-119422685	cassette	−0.27	−0.35
Gls	1.21	chr1:52244638-52244697	alt 3′ exon	−0.03	−0.3
Ogt	0.92	chrX:98838315-98838345	alt 3′ ss	−0.23	−0.3
Mapk9	1.08	chr11:49687766-49687837	mut ex	−0.14	−0.27
Robo2	0.95	chr16:74009020-74009031	cassette	−0.22	−0.23
2410002O22Rik	0.91	chr13:104942245-104942262	cassette	−0.28	−0.22
Uevld	1.35	chr7:54190253-54190410	cassette	−0.16	−0.2
Rapgef6	1.03	chr11:54507772-54508074	cassette	−0.12	−0.19
Sult4a1	1.12	chr15:83909199-83909327	cassette	−0.2	−0.18
Lrch3	0.99	chr16:32995892-32995999	cassette	−0.22	−0.18
Q8BLQ9-2	0.96	chr16:66731630-66731749	cassette	−0.29	−0.18
Dst	1.11	chr1:34306649-34306975	cassette	−0.15	−0.18
Vps29	1.04	chr5:122806803-122806814	cassette	−0.19	−0.17
Epb4.1	0.92	chr4:131518839-131518901	cassette/complex	−0.13	−0.17
Dhdds	0.95	chr4:133556254-133556308	alt 3′ ss	−0.17	−0.15
Abi1	1.06	chr2:22809128-22809131	alt 3′ ss	−0.09	−0.13
Macf1	1.05	chr4:123074337-123074663	cassette	−0.13	−0.11
Ank3	0.97	chr10:69416188-69416220	cassette	−0.07	−0.11
Rod1	1.02	chr4:59559021-59559054	cassette	−0.09	−0.08
Cadm3	1.13	chr1:175279153-175279254	cassette	−0.07	−0.06
Mdm2	0.96	chr10:117146774-117146840	cassette	−0.1	−0.06
2210010B09Rik	1.05	chr9:20393901-20394002	cassette	0.1	0.05
Cugbp2	0.97	chr2:6528928-6529007	cassette	0.08	0.06
Thyn1	0.93	chr9:26814386-26814536	cassette	0.14	0.06
Cldnd1	1.1	chr16:58729293-58729336	cassette	0.09	0.07
Nrxn1	1.06	chr17:91101328-91101351	cassette	0.06	0.09
Cltb	1.02	chr13:54698387-54698440	cassette	0.08	0.09
Ank2	1.04	chr3:126666301-126666399	cassette	0.09	0.11
Elavl2	0.86	chr4:90920832-90920870	cassette	0.06	0.12
Ap1gbp1	0.97	chr11:83853158-83853193	cassette	0.07	0.13
Kif2a	1.06	chr13:107759784-107759897	cassette	0.16	0.2
Snap25	1.07	chr2:136595479-136595596	mut ex	0.14	0.21
Mapk9	1.08	chr11:49687338-49687409	mut ex	0.13	0.27
Plekha5	0.84	chr6:140528868-140529056	cassette	0.25	0.28
Rufy2	1.29	chr10:62465694-62467405	alt 3′exon	0.32	0.37

Thirty-seven Elavl3/4-dependent alternative exons were experimentally verified by RT-PCR. ΔI values obtained from splicing microarray analysis and RT-PCR experiments are presented. A positive ΔI value is associated with a higher fraction of exon-included isoform in WT compared to DKO samples. Abbreviations: mut ex, mutually exclusive; alt 3′ exon, alternative 3′ exon; alt 3′ss, alternative 3′ splice site. See also Table S7.

analysis (|ΔI-rank| > 10; Table S8). Nine of these transcripts had zero tags in the alternative exons and the flanking regions and were excluded from further analysis as they might represent indirect effects or limited coverage of our CLIP data, since we do not believe that we have fully saturated nElavl binding sites in our HITS-CLIP data set. A total of 436 tags from the remaining 50 alternative exons were overlaid onto a composite pre-mRNA to generate a functional nElavl binding/splicing map (Figure 5A and Table S8). This map revealed that in a majority of cases nElavl binding sites were present in introns flanking the alternative exons and were most concentrated at exon/intron splice junctions.

In order to identify those binding sites that are most relevant to the alternative splicing events, a normalized complexity map representative of common nElavl binding regions in different pre-mRNAs was generated (Figure 5B), using strategies

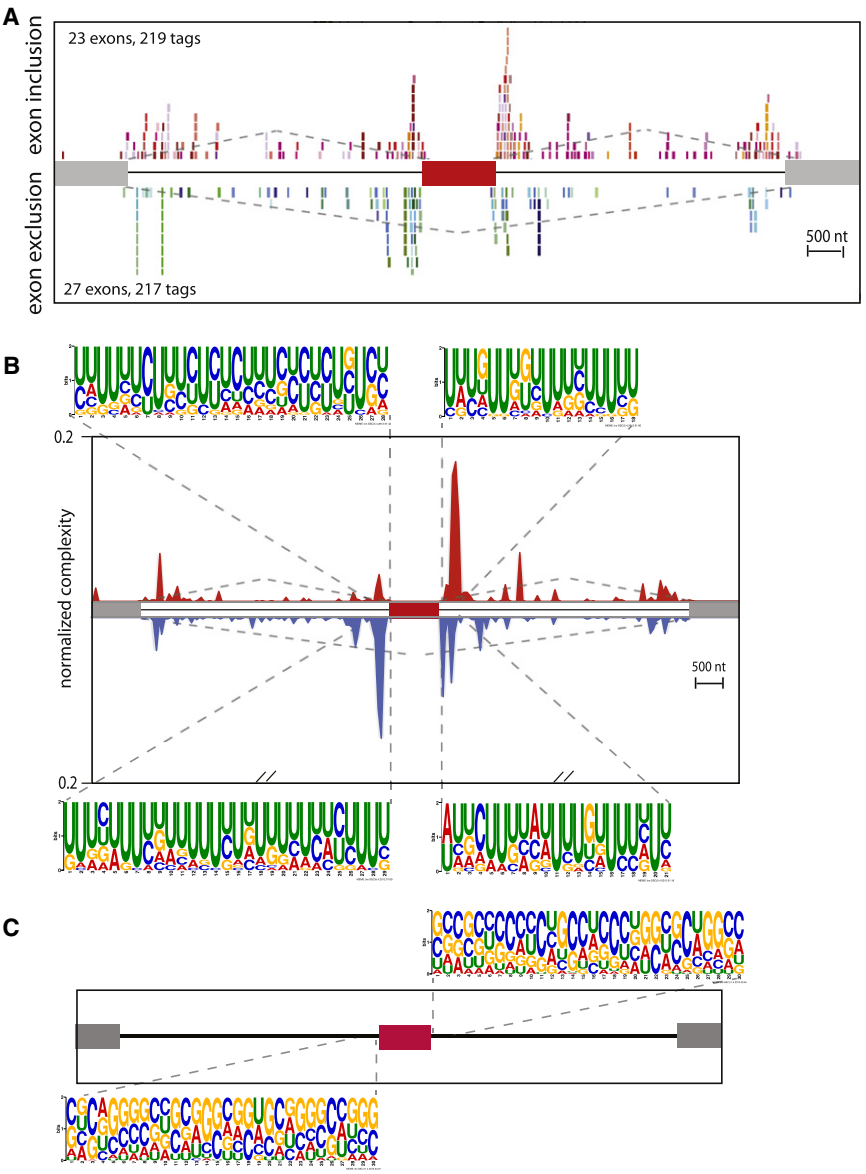

Figure 5. Normalized Complexity Map for nElavl-Dependent Alternative Splicing

(A) nElavl tags mapping to nElavl-regulated cassette exons or flanking introns are plotted onto a composite transcript as a function of distance to the 5′ or 3′ junctions of the alternative exon. Tags from independent CLIP experiments are color coded. Red and gray boxes represent a generic alternative cassette exon and flanking constitutive exons, respectively.

(B) Normalized complexity map of nElavl-dependent alternative splicing of cassette exons. Red and blue peaks represent binding associated with nElavl-dependent exon inclusion and exclusion, respectively. Motif preferences of 250 nt sequences flanking nElavl-regulated alternative exons are shown.

(C) Motif preferences of 250 nt sequences flanking randomly selected alternative exons that display no change in isoform abundance in DKO mice are shown.

See also Figure S2 and Table S8.

previously established for the neuronal splicing factor Nova (Licatalosi et al., 2008). The number of total nElavl-binding sites in 50 nt windows spanning a 12 kb region was normalized to the number of different transcripts displaying nElavl-binding in each window, to the number of total nElavl tags in individual pre-mRNAs and also to the number of independent experiments (biologic complexity) in which the tags in each cluster were identified. The results of this map revealed preferential nElavl binding to the 5′ splice site of the downstream intron in cassette exons where nElavl promotes inclusion and to the immediate 3′ and 5′ splice sites in those exons where nElavl promotes exclusion (Figure 5B). Furthermore, we observed a strong preference for U-rich sequences in flanking regions of nElavl-dependent exons and GC-rich sequences that were poor in U residues in flanking regions of nElavl-independent exons (Figures 5B and 5C). This data suggests that nElavl proteins preferentially regulate the alternative splicing of a specific subset of exons flanked by U-rich sequence motifs. Using the same data set we also mapped tag locations in individual nElavl pre-mRNA targets and consistently observed intronic binding within 250 nt of the exon/intron junctions in the flanking introns in nElavl suppressed and promoted alternative exons, respectively (Figure S2A). Taken together, our nElavl RNA map suggests a position-dependent splicing code for nElavl-regulated alternative cassette exon usage that is consistent with previously reported splicing factors.

Gene Ontology Analysis of nElavl Splicing Targets

To address the biological processes encoded by transcripts whose alternative splicing was regulated by nElavl, we carried out enrichment analysis for gene ontology (GO) categories on those transcripts that are nElavl-regulated at the alternative splicing level. For GO analysis the top 212 most significant target transcripts from our Aspire2 analysis results were used and compared to all genes expressed in WT brain (Table S10). These target alternative exon included not just cassette exons but also other modes of alternative splicing events regulated by nElavl. The nElavl-regulated transcripts that were the most significantly enriched overall encoded proteins involved in the regulation of protein complex and cytoskeleton dynamics, in particular microtubule polymerization and depolymerization activity at the synapse and axon (Table S11). For example, the top 10 enriched terms in biologic process (enriched 10- to 25-fold) all related to microtubule assembly/disassembly, in cellular component (enriched 1.9- to 22-fold, median 3.8) related to the synaptic cytoskeleton,

and in molecular function primarily related to regulation of microtubules and small GTPase mediated signaling (enriched 2.1- to 37-fold, median 2.9).

A Direct Role for nElavl Proteins in 3′UTR Regulation

The majority (63.5%) of robust nElavl binding sites (BC = 6) from HITS-CLIP data mapped onto 3′UTRs, suggesting that nElavl might have roles in the brain besides regulation of alternative splicing, such as maintenance of steady state mRNA levels. We investigated this possibility by first comparing total transcript levels in cortical tissue from WT and *Elavl3*$^{-/-}$;*Elavl4*$^{-/-}$ brains using Affymetrix exon microarrays. One hundred nineteen transcripts displayed significant changes in steady-state levels in DKO brain (two-tailed t test, p value < 0.01), with 89 transcripts decreased and 30 increased (Table S9).

To assess which of these transcripts might be directly regulated by nElavl binding in the 3′UTR, we assessed which had nElavl HITS-CLIP 3′UTR binding sites. Those transcripts whose abundance changed in DKO tissue had significantly more nElavl HITS-CLIP tags when compared to all expressed transcripts whose steady state levels were unaffected (p = 0.0037 by Wilcoxon rank-sum test; Figure S3). More specifically, we identified nElavl binding sites in 24 of the 89 transcripts whose abundance was decreased in DKO (Table S9).

A Role for nElavl in Regulating Glutamate in the Brain

GO analysis of the 119 transcripts whose steady-state was regulated by nElavl revealed a very different set of biologic processes than those encoded by transcripts whose splicing was regulated by nElavl. Transcripts whose steady-state levels were nElavl-regulated were enriched for genes regulating amino acid and sugar biosynthetic pathways (Table S11). Interestingly, the glutamine amino acid biosynthetic pathway was an outlier among GO biologic process enriched in nElavl-regulated steady-state transcripts (39-fold enrichment, p < 0.002). The genes in this pathway encode proteins catalyzing reactions that result in the formation of amino acids of the glutamine family, comprising glutamate, arginine, glutamine, and proline. Glutamate is the major excitatory neurotransmitter and also the biochemical precursor for the major inhibitory neurotransmitter GABA in the mammalian forebrain (Martin and Rimvall, 1993).

The marked enrichment for nElavl regulation of steady state mRNAs encoding the glutamine amino acid biosynthetic pathway prompted us to examine whether nElavl played a role in regulated glutamine synthesis in neurons. Measurement of total glutamate levels in extracts of cortical tissue from *Elavl3*$^{-/-}$;*Elavl4*$^{-/-}$ mice revealed approximately 50% reduction compared to WT littermates (Figure 6F).

The majority (70%) of neuronal glutamate is believed to be synthesized within neurons by glutaminase enzyme (encoded by Gls1/Gls gene) (Hertz and Zielke, 2004). Alternative usage of a 3′ exon during Gls1 pre-mRNA splicing results in the generation of two separate transcripts with different 3′ coding and UTR sequences, encoding for proteins harboring a short and a long C-terminal domain that we term Gls-s and Gls-l, respectively (Figure 6A). Interestingly, analysis of nElavl HITS-CLIP tags revealed nElavl binding sites on intronic sequences flanking the regulated alternative splice site, suggesting that nElavl might promote the alternative use of the isoform Gls1-l by binding to intronic regulatory sequences. We also observed that nElavl binds to the 3′UTR sequences of both isoforms (Figures 6A and S4). Thus, nElavl has the potential to regulate Gls1 isoform levels both at the AS and at the transcript abundance level.

The AS event generating the Gls-l and Gls-s isoforms was listed as a top target in our Aspire2 AS analysis, with a validated ΔI of −0.3, (Figure 6B and Table S7). Quantitative RT-PCR using primers specific for each Gls isoform demonstrated that in *Elavl3*$^{-/-}$;*Elavl4*$^{-/-}$ DKO brain, abundance of the Gls-s isoform did not change while abundance of the Gls1-l isoform was reduced to approximately 50% of the WT levels (Figure 6D). Western blot analysis using an antibody recognizing a common epitope to both isoforms also demonstrated that the abundance of Gls-s and Gls-l proteins were reduced to 60% and 25% of the WT levels, respectively (Figures 6C and 6E). Since *Elavl3/4* DKO die at age P0 it is difficult to further carry out any physiological analyses. We assessed whether *Elavl3*$^{-/-}$ single KO mice also exhibited a defect in glutamate regulation and observed a smaller but significant decrease in total glutamate levels and in Gls-l, but not Gls-s, protein levels (Figure S5). These results point to a role for nElavl proteins in directly controlling Gls-s and Gls-l levels in the nervous system through reinforcing mechanisms of involving both the regulation of AS and mRNA half-life, consistent with nElavl HITS-CLIP results demonstrating direct binding to both intronic and 3′UTR elements.

Seizures in *Elavl3*$^{-/-}$ Mice

To assess whether there might be a physiologic correlate of excitation/inhibition imbalance manifested by misregulation of glutamate signaling in *Elavl3*$^{-/-}$ mice, we undertook an EEG analysis of cortical function. Video EEG monitoring of awake and behaving mutants revealed a striking pattern of abnormal cortical hypersynchronization in both *Elavl3*$^{+/-}$ and *Elavl3*$^{-/-}$ mice never seen in WT mice (Figure 7A; Movie S1). In *Elavl3*$^{+/-}$ mice, there was a nearly continuous presence (1–9/min) of bilaterally synchronous sharp cortical spike discharges, sometimes accompanied by brief afterdischarges (Figure 7B). *Elavl3*$^{-/-}$ mice displayed similar discharges as well as more severe, non-convulsive electrographic seizures lasting from 10–30 s (Figure 7C). Both patterns demonstrate aberrant hypersynchronization in cortical networks.

DISCUSSION

Until recently studies aimed at identifying regulatory RNA sequences have been limited to correlative information lacking direct functional links to biological processes. HITS-CLIP technique provides a methodology to identify such functional RNA-protein interaction sites and has been successfully applied to identifying binding sites and uncovering new biological functions for several RNABPs, including Nova (Licatalosi et al., 2008), PTB (Xue et al., 2009), hnRNP C (König et al., 2010), TIA-1 (Wang et al., 2010b), TDP-43, and Fox2 (Yeo et al., 2009).

In the present study, we carried out unbiased genome-wide nElavl HITS-CLIP experiments in combination with microarray analysis using nElavl KO tissue and in vitro binding assays to identify functional interaction sites between neuronal nElavl

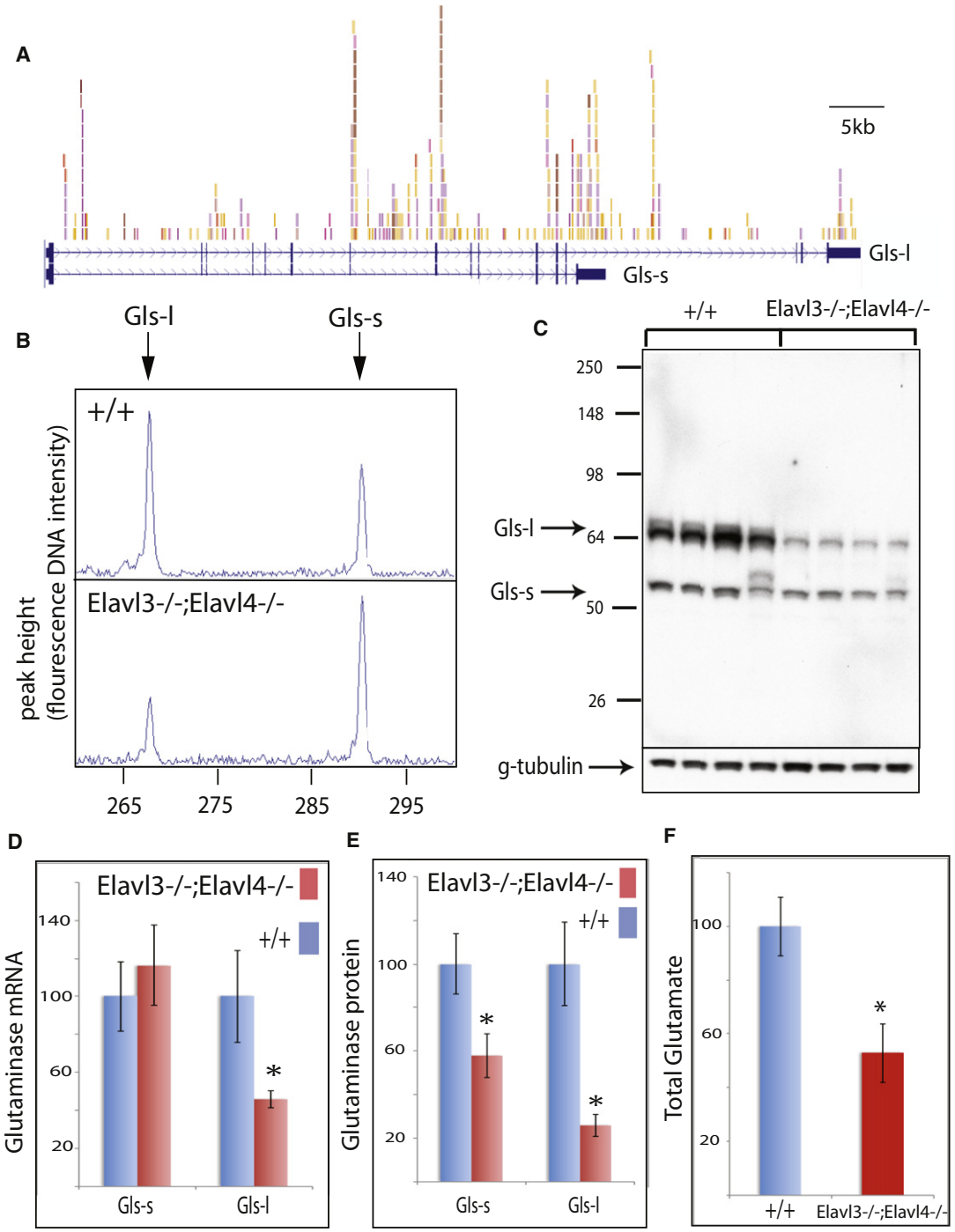

Figure 6. nElavl-Dependent Regulation of the Brain Enzyme Glutaminase

(A) The two mRNA isoforms of the glutaminase gene (Gls) and nElavl binding sites are shown. Individual colors depict different experiments. Alternative use of a 3′ splice site generates two Gls isoforms with different 3′ terminal coding sequences and 3′UTRs. Gls-s and Gls-l refer to short and long isoforms, respectively.

(B) RT-PCR amplification of the two Gls isoforms in WT and *Elavl3*$^{-/-}$;*Elavl4*$^{-/-}$ cortex of age P0 mice.

(C) Western blot analysis of the two Gls isoforms in littermate WT and *Elavl3*$^{-/-}$;*Elavl4*$^{-/-}$ cortex of age P0 mice. Each lane represents an independent mouse.

(D) Q-PCR quantification of the abundance of two Gls mRNA isoforms in littermate WT and *Elavl3*$^{-/-}$;*Elavl4*$^{-/-}$ cortex of age P0 mice.

(E) Quantification of data shown in (C) as normalized to gamma tubulin.

(F) Quantification of total glutamate levels in cortex of 3 WT and 3 *Elavl3*$^{-/-}$;*Elavl4*$^{-/-}$ littermate age P0 mice are presented. Glutamate levels in WT samples are normalized to 100% in the y axis. *$p < 0.01$ (t test). Error bars denote standard deviation.

See also Figures S3 and S4 and Table S9.

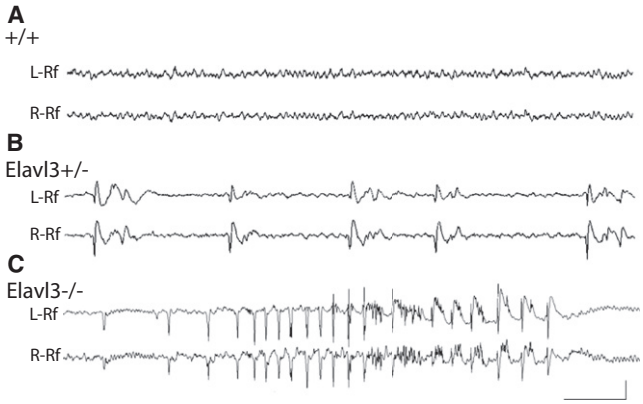

Figure 7. EEG Analysis of Cortical Function in *Elavl3*$^{-/-}$ Mice

Spontaneous bilateral EEG activity recorded from awake and behaving 3-to 6-month-old adult (A) WT, (B) *Elavl3*$^{+/-}$, and (C) *Elavl3*$^{-/-}$ mice. Cortical recordings are displayed from left (L-reference) and right (R-reference) hemisphere temporoparietal electrodes. WT mice lack abnormal discharges seen occurring intermittently in *Elavl3*$^{+/-}$ and *Elavl3*$^{-/-}$ mice. Brief seizures shown in *Elavl3*$^{-/-}$ mice are accompanied by mild convulsive clonic movements. Seizures were detected in both *Elavl3*$^{-/-}$ and *Elav3*$^{-/+}$ mice. Calibration, 1 s (A and C, 0.5 s in B), 200 microvolts (A–C). See also Figures S5 and S6, Tables S10 and 11, and Movie S1.

RNABPs and target RNA sequences. Our results demonstrate that nElavl RNABPs preferentially bind to U-rich sequences interspersed with purine residues (G > A) located on 3′UTRs and introns of target pre-mRNAs in the brain, which, taken together with previous studies, indicates two apparently independent functions of nElavl-RNA interactions. Specifically, we demonstrate that nElavl proteins bind to intronic sequences at flanking junctions of alternative exons on target pre-mRNAs, revealing an nElavl-RNA map associated with nElavl-dependent alternative splicing. We also find that by binding to 3′UTRs nElavl proteins regulate the steady state levels of distinct group of mRNAs. Interestingly, the observation of coordinate and mutually reinforcing actions of nElavl proteins on Gls-1 RNA suggest that its actions on pre-mRNA and mature mRNA can be functionally interrelated.

Nonetheless, analysis of the set of directly regulated transcripts suggests that nElavl proteins generally mediate different functional roles in different regulatory contexts. Transcripts regulated at the level of AS encode proteins involved in regulating cytoskeleton dynamics, particularly in synapses, while those regulated by 3′UTR binding encode a markedly different set of proteins involved in regulating basic biosynthetic pathways. This may make some evolutionary sense, as regulating alternative exon content alters the quality of proteins, while 3′UTR regulation alters their quantity, two very different outcomes under different sets of selective pressures. It will be of interest to determine whether such variable patterns of coordinate regulation are evident in the analysis of the direct targets of additional RNABPs.

To date, targets of nElavl proteins have been studied mainly using three approaches: in vitro RNA selection, relatively low-stringency immunoprecipitation of nElavl-RNA complexes (“RIP”) from cell lines followed by cDNA array hybridization of precipitated RNA and the study of candidate genes based on the presence of in vitro binding elements in their 3′UTRs in cultured cell lines. We compiled a list of 134 published targets of nElavl, which are largely identified bioinformatically and validated in vitro (Table S6). Most of these predicted targets were not validated by our HITS-CLIP analysis; only ~25% were identified (with an FDR < 1.0). Therefore, while these studies have led to determination of nElavl target sequence specificity and of numerous target mRNAs, whether they reflect nElavl-RNA interactions present in vivo in brain tissue remains uncertain. Moreover, a large number of RNA selection and in vitro binding studies report that nElavl proteins bind to AU-rich elements (Table S6). In vivo, we find that nElavl prefers to bind to related but distinct sites in the brain, consisting of U-rich stretches approximately 15–20 nt long interspersed with G residues. The nElavl binding motif we determine is in agreement with our independent in vitro RNA selection analysis, and with two immunoprecipitation and cDNA array studies where the binding preference for Elavl4 and the nonneuronally expressed Elavl1 paralog is reported as a GU rich stretch and a 20 nt long RNA motif rich in uracils, respectively (Bolognani et al., 2010; López de Silanes et al., 2004). These results reveal the utility of in vivo HITS-CLIP as a means of clarifying in vitro studies of RNA-protein interactions, which here initially led to the skewed perception that nElavl proteins bind only to ARE elements (Table S6). We find that nElavl proteins in fact bind GU-rich elements relative to ARE elements by ~1.3-fold and that it does so in clusters, analogous to the way in which Nova proteins recognize specific targets by binding clusters of low complexity YCAY elements (Licatalosi et al., 2008; Zhang et al., 2010).

nElav Regulation of Alternative Splicing

Previous studies in *Drosophila* have indicated that nElavl proteins are able to regulate alternative splicing (Koushika et al., 2000; Lisbin et al., 2001; Soller and White, 2003, 2005). Prior studies of mammalian nElavl splicing regulation has been less clear, as neither comparisons in genetically modified animals nor direct RNA binding assays have been previously employed. Here, we combined nElavl-RNA direct binding data with bioinformatics and exon junction array data comparing splicing in WT and KO animals to identify a definitive set of brain transcripts directly regulated by nElavl proteins in vivo. The results demonstrate that nElavl proteins directly bind neuronal pre-mRNA to regulate alternative splicing and that the proteins have redundant actions in this regard, as splicing changes were uniformly more pronounced in DKO than *Elavl3* or *Elavl4* single KO brain.

Our nElavl-RNA map is reminiscent of the position-dependence of splicing regulation observed for Nova, Fox2, hnRNP C, hnRNPL, TIA1/2, TDP-43, Mbnl, Ptbp1, and Ptbp2 and generally conforms to the finding that preferential binding to downstream introns leads to exon inclusion, and to upstream introns exon exclusion (Licatalosi et al., 2008, 2012; Llorian et al., 2010; Tollervey et al., 2011; Ule and Darnell, 2006; Yeo et al., 2009; Zhang et al., 2008). nElavl-mediated exon exclusion may be more frequently associated with binding to both upstream and downstream introns, a characteristic also noted for TDP-43 associated alternative splicing. As was also seen in the TDP-43 associated alternative splicing RNA-map, nElavl

binding was observed in deeper intronic sequences of a small number of cassette exons. Our nElavl-RNA map is also in agreement with several candidate target gene studies examining the role of nElavl proteins in AS. For example, it was recently demonstrated that Elavl3 promotes inclusion of the alternatively spliced exon 6 of the *Elavl4* gene by binding to U-rich sequences located in the intron downstream to the alternative exon (Wang et al., 2010a). Also, nElavl proteins suppress alternative exon 23a inclusion in the Neurofilament1 (*Nf1*) pre-mRNA by binding to U-rich intronic sequences on either intronic flanks of the cassette exon (Zhu et al., 2008). Our HITS-CLIP data indeed confirmed binding to two of the three nElavl target sequences reported in these studies (Figure S2B).

nElav Regulation of Neuronal Excitability

Our analysis of nElavl RNA targets revealed a reduction in levels of glutamate neurotransmitter in the brains of *Elavl3*$^{-/-}$;*Elavl4*$^{-/-}$ mice which corresponded to a decrease in Gls mRNA and protein levels. Currently, we do not exactly understand the mechanistic details of how nElavl proteins regulate the AS and mRNA stability of Gls mRNA isoforms. While mechanisms of post-transcriptional regulation of Gls-s and Gls-l mRNA are largely unknown in neurons, an mRNA stabilizing role for Elavl1 (HuA/R) binding to an AU-rich pH-responsive element located in the 3′UTR of Gls-l during metabolic acidosis in kidney cells is demonstrated (Ibrahim et al., 2008). It is also likely that nElavl proteins enhance the translation of at least the Gls-s isoform, since its mRNA levels are unaffected but proteins levels are significantly reduced in the *Elavl3*$^{-/-}$;*Elavl4*$^{-/-}$ brain tissue. The Gls is the major glutamate synthesizing enzyme in neurons. *Elavl3*$^{-/-}$;*Elavl4*$^{-/-}$ mice display some similarity to *Gls1*$^{-/-}$ mice, as both appear and behave normally at birth but die suddenly thereafter; in *Gls*$^{-/-}$ mice early postnatal death has been attributed to a deficiency in brain circuits controlling respiration (Masson et al., 2006). Glutamate is the major excitatory neurotransmitter and impacts inhibitory signaling in two ways: it is both the biochemical precursor for the major inhibitory neurotransmitter GABA in the mammalian forebrain (Martin and Rimvall, 1993), and synaptically activates inhibitory neuronal feedback loops (McBain and Fisahn, 2001). While the molecular lesion due to aberrant AS in this model is complex, imbalance of these key mediators of fast synaptic signaling in the *Elavl3*$^{-/-}$ brain is a well established mechanism for neuronal hypersynchrony and epilepsy (Noebels, 2003). The finding of abnormal hypersynchronization in both *Elavl3*$^{+/-}$ and *Elav3*$^{-/-}$ mice suggests that fine tuning of the stoichiometry of individual RNA isoforms can regulate cortical excitability and synchronization.

On the behavioral level, we observe attenuation of cerebellum-dependent motor function based on reduced rotarod assay performance in *Elavl3*$^{-/-}$ mice. Whether or not this behavioral defect results from reduced glutamatergic signaling and an imbalance in excitation/inhibition in the cerebellum are of great interest as future research questions.

Gls mRNA is alternatively spliced to generate two mRNA and protein isoforms, and the longer Gls-l isoform is dramatically reduced in both mRNA and protein levels in *Elavl3*$^{-/-}$;*Elavl4*$^{-/-}$ brain. Gls-s and Gls-l isoforms differ in their 3′UTR sequences and also C-terminal domains of their protein products. Both protein isoforms encode a glutaminase superfamily domain involved in deamination of glutamine to glutamate. Interestingly, four ankyrin repeat domains are present C-terminal to the glutaminase superfamily domain in Gls-l but not in the Gls-s isoforms. We suggest that nElavl regulates the protein interacting partners of this critical enzyme by maintaining a balance between the isoforms of the *Gls* gene.

Taken together, we establish nElavl proteins as regulators of neuron-specific AS, determine an nElavl-RNA map associated with alternative splicing and uncover a new nElavl-regulated biological pathway, namely the glutamate synthesis pathway. By investigating other nElavl targets our data set also offers the possibility of identifying other interesting functions of these neuronal proteins.

EXPERIMENTAL PROCEDURES

Generation of *Elav3* Targeting Construct for Homologous Recombination

A 17.7 kb targeting vector (see Supplemental Experimental Procedures) was selected in SV-129 ES cells, transferred into the germline of SV129/FVB mice, and the ACNF targeting cassette auto-excised in the male germ cells. All animal studies in this work were in accordance with the Code of Practice for the Housing and Care of Animals Used in Scientific Procedures, and was approved by the Rockefeller University Comparative Biosciences Center.

Western Blot, Immunofluorescence Microscopy, and Antibodies

Western blots were performed using 50 μg of cortex extract per lane. A pan anti-nElavl antibody (α-nElavl; paraneoplastic Hu antibody; RU IRB approved protocol 0148; patient code NA-0018, a 63-year-old with small cell lung cancer and Hu encephalomyelopathy who had a pan-sensory neuropathy expired from prolonged status epilepticus) was used for IF.

nElavl HITS CLIP

nElavl-RNA complexes in brain tissue were UV crosslinked and immunoprecipitated using specific human antisera. Isolated RNA molecules were reverse-transcribed, PCR amplified and sequenced on an Illumina GAIIx at the Rockefeller University Genomics Resource Center (see Supplemental Information).

Microarrays

Three and one-half micrograms of total RNA from *Elavl3*$^{-/-}$;*Elavl4*$^{-/-}$ and littermate WT P0 mice cortical tissue was reverse transcribed and sense target DNA was prepared as described in "GeneChip Whole-Transcript (WT) Sense Target Labeling Assay" protocol from Affymetrix. Labeled Target DNA was hybridized to GeneChip Mouse Exon 1.0 ST Array and to custom made Exon Junction Array (Affymetrix) at the Rockefeller University Genomics Resource Center.

RNA Isolation and Validation of nElavl Targets by RT-PCR

RT-PCR was used to validate alternative splicing changes as described (Licatalosi et al., 2008; Ule et al., 2005b). P0 cortex was dissected and immediately frozen in −80°C. RNA was isolated using Trizol plus RNA purification kit (Invitrogen). RNA was reverse transcribed using superscript III reverse transcriptase (Invitrogen). Abundance of RNA isoforms were determined by semi-quantitative RT-PCR or where indicated by quantitative PCR, respectively. The number of PCR cycles used was in the linear range of product amplification.

Measurement of Brain Glutaminase and Glutamate Levels

Rabbit anti-glutaminase antibody was courtesy of Norman Curthoys, Colorado State University. Cortex was dissected out at P0 and immediately frozen at −80°C. Tissue was then lysed in assay buffer for 10 min, spun down and supernatant was collected for measurements (Glutamate Assay Kit, Biovision). Glutamate levels were normalized to total protein levels as measured by Bradford assay.

Bioinformatics

See Supplemental Experimental Procedures.

Microarray Analysis

Mouse 1.0 ST exon array signals were analyzed using, X-ray (Biotique), Expression Console (Affymetrix) software, Excel, and Filemaker Pro programs. Exon junction microarray signals were analyzed using Aspire2 (Ule et al., 2005b).

nElavl HITS-CLIP Tag Sequence Analysis

Sequence reads (tags) were aligned to the mm9 build of the mouse genome. PCR duplicates were filtered out and unique tags were identified using the RefSeq reference database. Tag clusters were defined as at least two tags that have at least one overlapping base. Biologic complexity (BC) for a cluster was the number of independent CLIP experiments that have a tag in that cluster.

nElavl Consensus Sequence Analysis

The MEME-CHIP Suite was used for all motif analyses (Bailey and Elkan, 1994).

nElavl-RNA Alternative Splicing Map

The map was generated by calculating the distance of nElavl HITS-CLIP tags from exon/intron junctions of nElavl-regulated cassette exons and flanking constitutive exons. Normalized tag distances were mapped onto a composite nElavl AS map.

Gene Ontology Analysis

Top 119 transcripts ($p < 0.01$) obtained from analysis of Gene Chip Mouse Exon 1.0 ST Array and top 212 transcripts (dI-rank > |10|) obtained from analysis of Exon Junction Microarray Aspire2 results were used. Those transcripts whose abundance was above an expression level cutoff as determined by signal intensity from Mouse Exon 1.0ST Array results of WT samples were used as the background gene list. All GO analysis was done using DAVID Bioinformatics Resources 6.7 (Huang et al., 2009a, 2009b).

Video Electroencephalographic (vEEG) Recordings

Adult *Elavl3*$^{-/-}$, *Elavl3*$^{+/-}$, and unaffected WT littermate mice (aged 3–6 months) were surgically implanted for chronic cortical electroencephalography. Mice were anesthetized with Avertin (1.25% tribromoethanol/amyl alcohol solution, i.p.) using a dose of 0.02 ml/g. Teflon-coated silver wire electrodes (0.005 inch diameter) soldered to a microminiature connector were implanted bilaterally into the subdural space over temporal, parietal, and occipital cortices. Digital EEG activity was monitored daily for up to 2 weeks during prolonged overnight and random 3 hr sample recordings (Stellate Systems, Harmonie software version 6.1c). A video camera was used to monitor behavior during the EEG recording periods. All recordings were carried out at least 24 hr after surgery on mice freely moving in the test cage.

SUPPLEMENTAL INFORMATION

Supplemental Information includes six figures, eleven tables, one movie, and Supplemental Experimental Procedures and can be found with this article online at http://dx.doi.org/10.1016/j.neuron.2012.07.009.

ACKNOWLEDGMENTS

We thank members of the Darnell laboratory for advice and suggestions throughout the course of this work, Melis Kayikci for ASPIRE2 Analysis and Norman Curthoys for the glutaminase antibody. We are grateful to sources of support to GI-D (Rockefeller University, Women and Science Postdoctoral Fellowship), J.L.N. (NINDS NS 29709 and IDDRC HD24064), C.Z. (K99GM95713), R.B.D. (NS34389) and the Rockefeller University Hospital CTSA (UL1 RR024143). R.B.D. is an HHMI Investigator.

Accepted: July 5, 2012
Published: September 19, 2012

REFERENCES

Akamatsu, W., Fujihara, H., Mitsuhashi, T., Yano, M., Shibata, S., Hayakawa, Y., Okano, H.J., Sakakibara, S., Takano, H., Takano, T., et al. (2005). The RNA-binding protein HuD regulates neuronal cell identity and maturation. Proc. Natl. Acad. Sci. USA *102*, 4625–4630.

Bailey, T.L., and Elkan, C. (1994). Fitting a mixture model by expectation maximization to discover motifs in biopolymers. Proc. Int. Conf. Intell. Syst. Mol. Biol. *2*, 28–36.

Barash, Y., Calarco, J.A., Gao, W., Pan, Q., Wang, X., Shai, O., Blencowe, B.J., and Frey, B.J. (2010). Deciphering the splicing code. Nature *465*, 53–59.

Bolognani, F., Contente-Cuomo, T., and Perrone-Bizzozero, N.I. (2010). Novel recognition motifs and biological functions of the RNA-binding protein HuD revealed by genome-wide identification of its targets. Nucleic Acids Res. *38*, 117–130.

Brennan, C.M., and Steitz, J.A. (2001). HuR and mRNA stability. Cell. Mol. Life Sci. *58*, 266–277.

Buckanovich, R.J., and Darnell, R.B. (1997). The neuronal RNA binding protein Nova-1 recognizes specific RNA targets in vitro and in vivo. Mol. Cell. Biol. *17*, 3194–3201.

Calarco, J.A., Zhen, M., and Blencowe, B.J. (2011). Networking in a global world: establishing functional connections between neural splicing regulators and their target transcripts. RNA *17*, 775–791.

Castle, J.C., Zhang, C., Shah, J.K., Kulkarni, A.V., Kalsotra, A., Cooper, T.A., and Johnson, J.M. (2008). Expression of 24,426 human alternative splicing events and predicted cis regulation in 48 tissues and cell lines. Nat. Genet. *40*, 1416–1425.

Darnell, R.B. (2010). HITS-CLIP: panoramic views of protein-RNA regulation in living cells. Wiley Interdiscip. Rev. RNA *1*, 266–286.

Darnell, J.C., Van Driesche, S.J., Zhang, C., Hung, K.Y., Mele, A., Fraser, C.E., Stone, E.F., Chen, C., Fak, J.J., Chi, S.W., et al. (2011). FMRP stalls ribosomal translocation on mRNAs linked to synaptic function and autism. Cell *146*, 247–261.

Das, D., Clark, T.A., Schweitzer, A., Yamamoto, M., Marr, H., Arribere, J., Minovitsky, S., Poliakov, A., Dubchak, I., Blume, J.E., and Conboy, J.G. (2007). A correlation with exon expression approach to identify cis-regulatory elements for tissue-specific alternative splicing. Nucleic Acids Res. *35*, 4845–4857.

Hertz, L., and Zielke, H.R. (2004). Astrocytic control of glutamatergic activity: astrocytes as stars of the show. Trends Neurosci. *27*, 735–743.

Hinman, M.N., and Lou, H. (2008). Diverse molecular functions of Hu proteins. Cell. Mol. Life Sci. *65*, 3168–3181.

Huang, C.S., Shi, S.H., Ule, J., Ruggiu, M., Barker, L.A., Darnell, R.B., Jan, Y.N., and Jan, L.Y. (2005). Common molecular pathways mediate long-term potentiation of synaptic excitation and slow synaptic inhibition. Cell *123*, 105–118.

Huang, W., Sherman, B.T., and Lempicki, R.A. (2009a). Bioinformatics enrichment tools: paths toward the comprehensive functional analysis of large gene lists. Nucleic Acids Res. *37*, 1–13.

Huang, W., Sherman, B.T., and Lempicki, R.A. (2009b). Systematic and integrative analysis of large gene lists using DAVID bioinformatics resources. Nat. Protoc. *4*, 44–57.

Ibrahim, H., Lee, Y.J., and Curthoys, N.P. (2008). Renal response to metabolic acidosis: role of mRNA stabilization. Kidney Int. *73*, 11–18.

Jensen, K.B., and Darnell, R.B. (2008). CLIP: crosslinking and immunoprecipitation of in vivo RNA targets of RNA-binding proteins. Methods Mol. Biol. *488*, 85–98.

König, J., Zarnack, K., Rot, G., Curk, T., Kayikci, M., Zupan, B., Turner, D.J., Luscombe, N.M., and Ule, J. (2010). iCLIP reveals the function of hnRNP particles in splicing at individual nucleotide resolution. Nat. Struct. Mol. Biol. *17*, 909–915.

Koushika, S.P., Lisbin, M.J., and White, K. (1996). ELAV, a *Drosophila* neuron-specific protein, mediates the generation of an alternatively spliced neural protein isoform. Curr. Biol. *6*, 1634–1641.

Koushika, S.P., Soller, M., and White, K. (2000). The neuron-enriched splicing pattern of Drosophila erect wing is dependent on the presence of ELAV protein. Mol. Cell. Biol. *20*, 1836–1845.

Lebedeva, S., Jens, M., Theil, K., Schwanhäusser, B., Selbach, M., Landthaler, M., and Rajewsky, N. (2011). Transcriptome-wide analysis of regulatory interactions of the RNA-binding protein HuR. Mol. Cell *43*, 340–352.

Li, Q., Lee, J.A., and Black, D.L. (2007). Neuronal regulation of alternative pre-mRNA splicing. Nat. Rev. Neurosci. *8*, 819–831.

Li, J.B., Levanon, E.Y., Yoon, J.K., Aach, J., Xie, B., Leproust, E., Zhang, K., Gao, Y., and Church, G.M. (2009). Genome-wide identification of human RNA editing sites by parallel DNA capturing and sequencing. Science *324*, 1210–1213.

Licatalosi, D.D., and Darnell, R.B. (2010). RNA processing and its regulation: global insights into biological networks. Nat. Rev. Genet. *11*, 75–87.

Licatalosi, D.D., Mele, A., Fak, J.J., Ule, J., Kayikci, M., Chi, S.W., Clark, T.A., Schweitzer, A.C., Blume, J.E., Wang, X., et al. (2008). HITS-CLIP yields genome-wide insights into brain alternative RNA processing. Nature *456*, 464–469.

Licatalosi, D.D., Yano, M., Fak, J.J., Mele, A., Grabinski, S.E., Zhang, C., and Darnell, R.B. (2012). Ptbp2 represses adult-specific splicing to regulate the generation of neuronal precursors in the embryonic brain. Genes Dev. *26*, 1626–1642.

Lisbin, M.J., Qiu, J., and White, K. (2001). The neuron-specific RNA-binding protein ELAV regulates neuroglian alternative splicing in neurons and binds directly to its pre-mRNA. Genes Dev. *15*, 2546–2561.

Llorian, M., Schwartz, S., Clark, T.A., Hollander, D., Tan, L.Y., Spellman, R., Gordon, A., Schweitzer, A.C., de la Grange, P., Ast, G., and Smith, C.W. (2010). Position-dependent alternative splicing activity revealed by global profiling of alternative splicing events regulated by PTB. Nat. Struct. Mol. Biol. *17*, 1114–1123.

López de Silanes, I., Zhan, M., Lal, A., Yang, X., and Gorospe, M. (2004). Identification of a target RNA motif for RNA-binding protein HuR. Proc. Natl. Acad. Sci. USA *101*, 2987–2992.

Martin, D.L., and Rimvall, K. (1993). Regulation of gamma-aminobutyric acid synthesis in the brain. J. Neurochem. *60*, 395–407.

Masson, J., Darmon, M., Conjard, A., Chuhma, N., Ropert, N., Thoby-Brisson, M., Foutz, A.S., Parrot, S., Miller, G.M., Jorisch, R., et al. (2006). Mice lacking brain/kidney phosphate-activated glutaminase have impaired glutamatergic synaptic transmission, altered breathing, disorganized goal-directed behavior and die shortly after birth. J. Neurosci. *26*, 4660–4671.

McBain, C.J., and Fisahn, A. (2001). Interneurons unbound. Nat. Rev. Neurosci. *2*, 11–23.

McKee, A.E., Minet, E., Stern, C., Riahi, S., Stiles, C.D., and Silver, P.A. (2005). A genome-wide in situ hybridization map of RNA-binding proteins reveals anatomically restricted expression in the developing mouse brain. BMC Dev. Biol. *5*, 14.

Mukherjee, N., Corcoran, D.L., Nusbaum, J.D., Reid, D.W., Georgiev, S., Hafner, M., Ascano, M., Jr., Tuschl, T., Ohler, U., and Keene, J.D. (2011). Integrative regulatory mapping indicates that the RNA-binding protein HuR couples pre-mRNA processing and mRNA stability. Mol. Cell *43*, 327–339.

Noebels, J.L. (2003). The biology of epilepsy genes. Annu. Rev. Neurosci. *26*, 599–625.

Okano, H.J., and Darnell, R.B. (1997). A hierarchy of Hu RNA binding proteins in developing and adult neurons. J. Neurosci. *17*, 3024–3037.

Pan, Q., Shai, O., Lee, L.J., Frey, B.J., and Blencowe, B.J. (2008). Deep surveying of alternative splicing complexity in the human transcriptome by high-throughput sequencing. Nat. Genet. *40*, 1413–1415.

Ruggiu, M., Herbst, R., Kim, N., Jevsek, M., Fak, J.J., Mann, M.A., Fischbach, G., Burden, S.J., and Darnell, R.B. (2009). Rescuing Z+ agrin splicing in Nova null mice restores synapse formation and unmasks a physiologic defect in motor neuron firing. Proc. Natl. Acad. Sci. USA *106*, 3513–3518.

Soller, M., and White, K. (2003). ELAV inhibits 3′-end processing to promote neural splicing of ewg pre-mRNA. Genes Dev. *17*, 2526–2538.

Soller, M., and White, K. (2005). ELAV multimerizes on conserved AU4-6 motifs important for ewg splicing regulation. Mol. Cell. Biol. *25*, 7580–7591.

Szabo, A., Dalmau, J., Manley, G., Rosenfeld, M., Wong, E., Henson, J., Posner, J.B., and Furneaux, H.M. (1991). HuD, a paraneoplastic encephalomyelitis antigen, contains RNA-binding domains and is homologous to Elav and Sex-lethal. Cell *67*, 325–333.

Tollervey, J.R., Curk, T., Rogelj, B., Briese, M., Cereda, M., Kayikci, M., König, J., Hortobágyi, T., Nishimura, A.L., Zupunski, V., et al. (2011). Characterizing the RNA targets and position-dependent splicing regulation by TDP-43. Nat. Neurosci. *14*, 452–458.

Ule, J., and Darnell, R.B. (2006). RNA binding proteins and the regulation of neuronal synaptic plasticity. Curr. Opin. Neurobiol. *16*, 102–110.

Ule, J., Jensen, K.B., Ruggiu, M., Mele, A., Ule, A., and Darnell, R.B. (2003). CLIP identifies Nova-regulated RNA networks in the brain. Science *302*, 1212–1215.

Ule, J., Jensen, K., Mele, A., and Darnell, R.B. (2005a). CLIP: a method for identifying protein-RNA interaction sites in living cells. Methods *37*, 376–386.

Ule, J., Ule, A., Spencer, J., Williams, A., Hu, J.S., Cline, M., Wang, H., Clark, T., Fraser, C., Ruggiu, M., et al. (2005b). Nova regulates brain-specific splicing to shape the synapse. Nat. Genet. *37*, 844–852.

Ule, J., Stefani, G., Mele, A., Ruggiu, M., Wang, X., Taneri, B., Gaasterland, T., Blencowe, B.J., and Darnell, R.B. (2006). An RNA map predicting Nova-dependent splicing regulation. Nature *444*, 580–586.

Wang, J., and Bell, L.R. (1994). The Sex-lethal amino terminus mediates cooperative interactions in RNA binding and is essential for splicing regulation. Genes Dev. *8*, 2072–2085.

Wang, E.T., Sandberg, R., Luo, S., Khrebtukova, I., Zhang, L., Mayr, C., Kingsmore, S.F., Schroth, G.P., and Burge, C.B. (2008). Alternative isoform regulation in human tissue transcriptomes. Nature *456*, 470–476.

Wang, H., Molfenter, J., Zhu, H., and Lou, H. (2010a). Promotion of exon 6 inclusion in HuD pre-mRNA by Hu protein family members. Nucleic Acids Res. *38*, 3760–3770.

Wang, Z., Kayikci, M., Briese, M., Zarnack, K., Luscombe, N.M., Rot, G., Zupan, B., Curk, T., and Ule, J. (2010b). iCLIP predicts the dual splicing effects of TIA-RNA interactions. PLoS Biol. *8*, e1000530.

Xue, Y., Zhou, Y., Wu, T., Zhu, T., Ji, X., Kwon, Y.S., Zhang, C., Yeo, G., Black, D.L., Sun, H., et al. (2009). Genome-wide analysis of PTB-RNA interactions reveals a strategy used by the general splicing repressor to modulate exon inclusion or skipping. Mol. Cell *36*, 996–1006.

Yano, M., Hayakawa-Yano, Y., Mele, A., and Darnell, R.B. (2010). Nova2 regulates neuronal migration through an RNA switch in disabled-1 signaling. Neuron *66*, 848–858.

Yeo, G.W., Coufal, N.G., Liang, T.Y., Peng, G.E., Fu, X.D., and Gage, F.H. (2009). An RNA code for the FOX2 splicing regulator revealed by mapping RNA-protein interactions in stem cells. Nat. Struct. Mol. Biol. *16*, 130–137.

Zhang, C., Zhang, Z., Castle, J., Sun, S., Johnson, J., Krainer, A.R., and Zhang, M.Q. (2008). Defining the regulatory network of the tissue-specific splicing factors Fox-1 and Fox-2. Genes Dev. *22*, 2550–2563.

Zhang, C., Frias, M.A., Mele, A., Ruggiu, M., Eom, T., Marney, C.B., Wang, H., Licatalosi, D.D., Fak, J.J., and Darnell, R.B. (2010). Integrative modeling defines the Nova splicing-regulatory network and its combinatorial controls. Science *329*, 439–443.

Zhu, H., Hinman, M.N., Hasman, R.A., Mehta, P., and Lou, H. (2008). Regulation of neuron-specific alternative splicing of neurofibromatosis type 1 pre-mRNA. Mol. Cell. Biol. *28*, 1240–1251.